N91-22995

AN EFFICIENT AND ACCURATE TECHNIQUE TO COMPUTE THE ABSORPTION, EMISSION, AND TRANSMISSION OF RADIATION BY THE MARTIAN ATMOSPHERE. Bernhard Lee Lindner, AER Inc., 840 Memorial Drive, Cambridge, MA 02139; Thomas P. Ackerman, Dept. of Meteor., Penn. State Univ., University Park, PA 16802; and James B. Pollack, NASA/ARC, Moffett Field, CA 94035.

INTRODUCTION. CO_2 comprises 95% of the composition of the martian atmosphere [1]. However, the martian atmosphere also has a high aerosol content. Dust opacities vary from less than 0.2 to greater than 3.0, primarily on a seasonal basis with the occurrence of global dust storms during southern spring [2]. Ice-cloud opacities vary from 0 to greater than 1, with large amounts occurring at winter polar latitudes [3]. CO_2 is an active absorber and emitter in near-IR and IR wavelengths; the near-IR absorption bands of CO_2 provide significant heating of the atmosphere, and the 15 μm band provides rapid cooling[4-7]. However, dust and ice-cloud aerosols have high scattering albedoes in solar wavelengths, and are highly absorbing at infrared wavelengths, and are as important as CO_2 in the atmospheric energy budget [5].

Including both CO_2 and aerosol radiative transfer simultaneously in a model is difficult. Aerosol radiative transfer requires a multiple-scattering code, while CO_2 radiative transfer must deal with complex wavelength structure, as shown in Fig. 1. The problem can be solved exactly by inserting the CO_2 absorptance for each spectral line into a multiple-scattering code, but the 15μm band alone has on the order of 10,000 lines, making such a computation tedious and expensive. It is this difficulty of simultaneously treating aerosol multiple scattering and the banded absorption structure of CO_2 that prompts most radiative-transfer studies of the martian atmosphere to consider either a pure-CO_2 or pure-dust atmosphere. This approximation simplifies treatment, but is inaccurate.

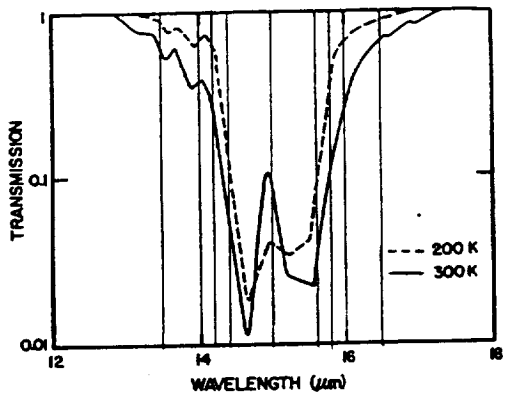

Figure 1. CO_2 15 μm band transmission at 20 km altitude looking upward, at temperatures of 200 and 300K [25]. Also shown are the sub-intervals used for the 8 term and 16 term fits.

One alternative technique that has recently been developed for atmospheric applications is the exponential-sum or k-distribution approximation [8-21]. The transmission of a homogeneous atmosphere is actually independent of the ordering of the absorption coefficient, k, in frequency space within a spectral interval, depending only upon the percentage of the spectral interval that has a particular value of k. The percentage of the spectral interval which has values between k and k + Δk can be formulated in a probability density function f(k) shown schematically in Fig. 2. The chief advantage of the exponential-sum approach is that the integration over k space of f(k) can be computed more quickly than the integration of k_ν over frequency. The exponential-sum approach is superior to the photon-path-distribution and emissivity techniques for dusty conditions [22, 19, 23]. Our work is the first application of the exponential-sum approach to martian conditions.

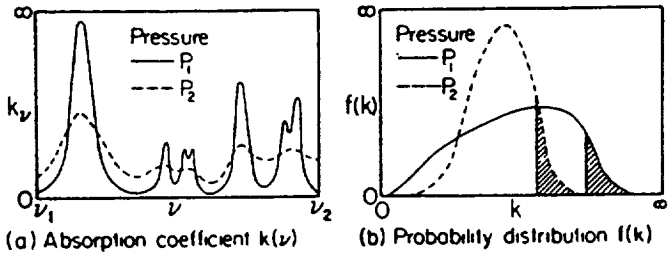

Figure 2. A schematic illustration portraying the essence of the exponential-sum approach. (a) shows a schematic of absorption line spectra at two different pressures. In (b) the two probability density functions f(k) associated with (a) are illustrated. The shaded area depicts the strongest absorption (i.e., largest k) for the same spectral interval (i.e., f(k) for different pressures are correlated). Integration of f(k) over k replaces the integration of k_ν over ν (modified from [28], [29]).

THEORETICAL APPROACH. The transmittance of the 15 μm band and the near-IR bands of CO_2 was computed using the FASCOD line-by-line transmittance model [24], modified for martian conditions. Computations with the modified FASCOD model were made at 3 temperatures (125K, 200K, 300K) and 5 pressures (100 mb, 10 mb, 1 mb, 0.1 mb, 0.01 mb); these cover the range of temperature and pressure currently observed in the atmosphere at all latitudes, seasons, and altitudes up to 40 km, and also can be used for early Mars, dense atmosphere studies. The near-IR and 15μm bands were broken into spectral sub-intervals (see Fig. 1), and the

transmittance for each layer, Tr, as a function of CO_2 column abundance within that layer, u, was fit with a series of weighting coefficients, a_i, and exponential coefficients, b_i:

$$Tr(u) \simeq \sum_{i=1}^{n} a_i \exp(-b_i u) \quad (1)$$

We tried fitting procedures based on Wiscombe and Evans [14] and an improved version of Ackerman et al. [13], and found both yielded similar results. Both of these procedures avoid the ill-conditioning of earlier exponential-sum routines, and produce more accurate and unique solutions [13,14]. The exponential-sum fit reproduced the FASCOD transmittances to better than 10^{-4} for all CO_2 abundances considered. The frequency sub-intervals are picked to try to minimize the variation in line strengths within the sub-interval. As shown in Fig. 1, 2 sub-intervals covered the band center, 2 covered the far line wings, 2 covered the near line wings, and 2 covered the transition from wings to band center. The vertical inhomogeneity of the atmosphere is treated by using homogeneous layers, with the absorption coefficients k for all layers correlated in frequency space, i.e. the sub-intervals of the spectral band which have the maximum absorption also have the largest k values (Ackerman et al., 1976). An interpolation is used for temperatures and pressures which fall in between the values at which the exponential-sum coefficients were computed. We compared a logarithmic interpolation to a linear interpolation, and found the logarithmic interpolation to be more accurate.

INCORPORATION IN MULTIPLE-SCATTERING MODELS. Vertical optical depths of CO_2 absorption for each term number, frequency sub-interval, and atmospheric layer are $b_i u$. CO_2 is combined with dust and cloud in that the total optical depth T_i, single-scattering albedo $\tilde{\omega}_i$, and phase function P for each term, frequency sub-interval, and layer are given by[16]:

$$T_i = b_i u + \tau^R + \tau_s^D + \tau_a^D + \tau_s^C + \tau_a^C \quad (2)$$

$$\tilde{\omega}_i = (\tau^R + \tau_s^D + \tau_s^C) / T_i \quad (3)$$

$$P = \frac{\tau_s^D P^D + \tau_s^C P^C + \tau^R P^R}{\tau_s^D + \tau_s^C + \tau^R} \quad (4)$$

where: τ^R - Rayleigh scattering optical depth for that layer

$\tau_{s,a}^{D,C}$ - Dust (D) and Cloud (C) scattering (s) and absorption (a) optical depth for that layer

$P^{D,C,R}$ - dust (D), cloud (C), and Rayleigh scattering (R) phase function

The multiple-scattering code is run once for each term in the sum using the T, $\tilde{\omega}_i$, and P appropriate to that term, and the resultant fluxes, F_i, (or intensities) are then summed and weighted by a_i to give the total flux, F, (or intensity) over the frequency sub-interval:

$$F = \sum_{i=1}^{n} a_i F_i(b_i u) \quad (5)$$

Tables of the exponential-sum coefficients, a_i and b_i, can be obtained from the authors.

NUMERICAL STUDIES. The number of terms in the series of exponentials (n in equation 1) and the number of sub-intervals into which the spectral band is broken can be varied to increase the desired accuracy. Figure 3 shows a comparison between the 15 μm cooling rates computed using various numbers of frequency sub-intervals and terms within each sub-interval. The temperature of the atmospheric model rose linearly from 150K at the surface to 160K at 10km altitude, and then fell linearly to 130K at 40km altitude. These temperatures are typical of the winter polar atmosphere on Mars. Using 4 terms and 4 sub-intervals results in an error of less than 10% in the lowest 10 km, but results in substantial errors at higher altitudes. The explanation is that the 4 term fit could not capture the effects of both the band center and the wings at all altitudes, and in this case we emphasized the wings, which are more important at lower altitudes where the band center is saturated (see Fig. 1). Adding additional terms from 8 to 16 is far less noticeable.

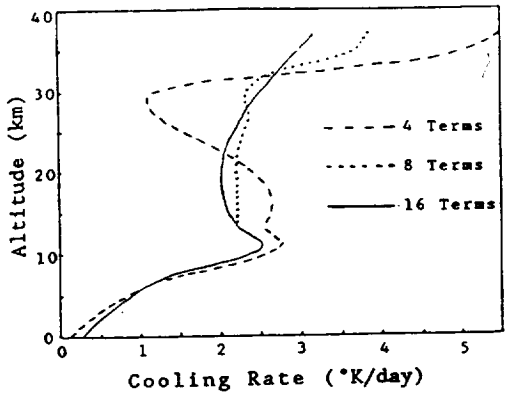

Figure 3. 15 μm band cooling rates calculated with an exponential-sum approach using 4 frequency sub-intervals and 4 terms in the sum, 10 sub-intervals and 8 terms, and 10 sub-intervals and 16 terms. A winter polar temperature profile is used (see text), but only 200K exponential-sum coefficients are used for comparison purposes.

We also separately derived exponential-sum coefficients based on the Gal'tsev and Osipov [25] line-by-line calculations of the 15 μm band. The number of terms in the fit (n in equation 1) were varied, to confirm our FASCOD work on the number of terms required to give an accurate fit. Figure 4 shows cooling rates computed with several fits to the Gal'tsev and Osipov parameterizations, as well as to the FASCOD transmittances. Cooling rates compare favorably in the lower atmosphere (below 10 km altitude). Gal'tsev and Osipov only considered temperatures as cold as 200K. We extrapolated the temperature dependence to colder temperatures [26]. Discrepancies between the Gal'tsev and Osipov and FASCOD cooling rates are due to the inaccuracy in the temperature extrapolation, particularly at the higher, colder altitudes. Again, note that the 4 and 5 term fits become inaccurate above 10 km altitude, as in Fig. 3. Also, the 15 term fit yields no marked improvement over the 8 term fit, as also shown with the FASCOD fits in Fig. 3.

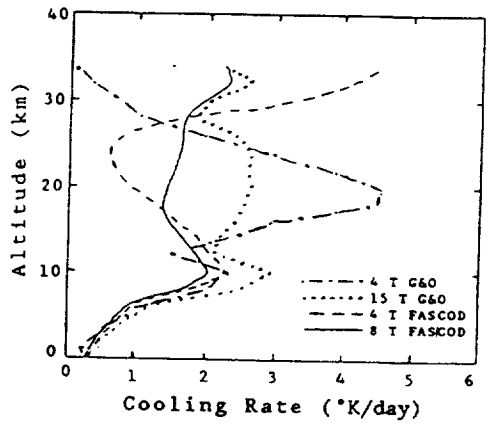

Figure 4. 15 μm band cooling rates calculated with 4 types of exponential-sum coefficients: 4 and 15 term fits to the transmission parameterizations of [25] (abbrev. G&O), and 4 and 8 term fits to the FASCOD transmission model. The winter polar atmosphere model is used, with logarithmic temperature interpolation for the exponential coefficients.

Cooling rates computed using the FASCOD exponential-sum transmittances also compared well below 10 km altitude with cooling rates computed using the Pollack et al. [27,4] parameterizations of CO_2 transmittance. At higher altitudes, discrepancies exist due to the use of the strong-line approximation by Pollack et al, which emphasizes the effects of the line wings. However, comparisons of our exponential-sum transmittances with techniques commonly used for the terrestrial atmosphere have indicated that our exponential-sum transmittances could be in error above 20 km altitude. J. Pollack is seeking to modify our exponential-sum approach to use two sets of sums, one applied to the line centers and one applied to the line wings. Initial tests seem to show better agreement in the upper atmosphere of Mars.

B.L. Lindner acknowledges support by NASA contract NASW-4444.

REFERENCES. [1]Owen, T. et al., J. Geophys. Res., 82, 4635, 1977. [2]Pollack, J. et al., J. Geophys. Res., 84, 2929, 1979. [3]Briggs, G. and C. Leovy, Bull. Amer. Met. Soc., 55, 278, 1974. [4]Gierasch, P. and R. Goody, Planet. Space. Sci., 15, 1465, 1967. [5]Kondratyev, K. et al., Sov. Phys. Dokl., 24, 81, 1979. [6]Pollack, J. et al., J. Atmos. Sci., 38, 3, 1981. [7]Lindner, B.L., The aeronomy and radiative transfer of the martian atmosphere, Ph.D. Dissertation, 470 pp., University of Colorado, Boulder, 1985. [8]Kondratyev, K., Radiation in the Atmosphere, Academic Press, 1969. [9]Arking, A. and K. Grossman, J. Atmos. Sci., 29, 937, 1972. [10]Raschke, E. and U. Stucke, Beitr. Phys. Atmosph., 46, 203, 1973. [11]Liou, K. and T. Sasamori, J. Atmos. Sci., 32, 2166, 1975. [12]Kerschgens, M. et al., Beitr. Phys. Atmosph., 49, 81, 1976. [13]Ackerman, T. et al., J. App. Meteor., 15, 28, 1976. [14]Wiscombe, W. and J. Evans, J. Computational Phys., 24, 416, 1977. [15]Morcrete, J., Beitr. Phys. Atmosph., 51, 338, 1978. [16]Freeman, K. and K. Liou, Adv. Geophys., 21, 231, 1979. [17]Evans, J. et al., Math. of Computat., 34, 203, 1980. [18]Chou, M. and A. Arking, J. Atmos. Sci., 38, 798, 1981. [19]Zdunkowski, W. et al., Beitr. Phys. Atmos., 55, 215, 1982. [20]Slingo, A. and H. Schrecker, Quart. J. R. Met. Soc., 108, 407, 1982. [21]Wang, W. and G. Shi, J. Quant. Spectrosc. Radiat. Transfer, 39, 387, 1988. [22]Bakan, S. et al., Beitr. Phys. Atmosph., 51, 28, 1978. [23]Wiscombe, W., Rev. Geophys. Space Phys., 21, 997, 1983. [24]Clough, S. et al., Proceedings of the Sixth Conference on Atmospheric Radiation, Williamsburg, VA, 1986. [25]Gal'tsev, A. and V. Osipov, Bull. (Izv.) Acad. Sci. USSR. Atmos. Ocean. Phys., 15, 767, 1979. [26]Lindner, B.L., The martian polar cap: Radiative effects of ozone, clouds, and airborne dust, J. Geophys. Res., 95, 1367, 1990. [27]Pollack, J. et al., Geophys. Res. Lett., 3, 479, 1976. [28]Stephens, G., Mon. Wea. Rev., 112, 826, 1984. [29] Hansen, J. et al., Mon. Wea. Rev., 111, 609, 1983.

MAGMATIC PROCESSES ON MARS: INSIGHTS FROM SNC METEORITES;

J. Longhi, Lamont-Doherty Geological Observatory, Palisades, NY 10964 .

The composition and petrology of the SNC (shergottites-nakhlites-Chassigny) meteorites reveal a surprising diversity of magmatic processes on their parent body, which the weight of evidence suggests is Mars (1). There is evidence for large scale mantle heterogeneities, multi-stage melting, extreme fractionation of REE, assimilation of a long-term light REE-enriched component (a 'granitic' crust?), mantle metasomatism, and possibly CO_2-fluxed melting. In some respects the style of martian magmatism is intermediate between that of the Moon and the Earth, with the terrestrial component having some of the geochemical character of hot-spot and arc basalts.

Estimates of the major element composition of the SNC parent magmas show them to be hpyersthene-normative, high-Fe, low-Al liquids (2). As might be anticipated, calculated densities of these liquids are high (2.75-2.96) and viscosities are low (4-128 poise). These compositions are consistent with the petrography: olivine and pyroxene crystallize early, plagioclase crystallizes late (1); this crystallization pattern is different from terrestrial MORB's and continental tholeiites in which plagioclase crystallizes early. These low-Al liquids require either large degrees (~50%) of partial melting of an undepleted source or smaller degrees of melting of a depleted source. Geochemical and isotopic data discussed below show the latter certainly to be the case for Nakhla and probably to be the case for the shergottites. This depletion may be accomplished by the accumulation of olivine and pyroxene (lunar style) or extraction of basalt (terrestrial style).

Figure 1 illustrates some important aspects of SNC trace element and isotopic composition. Figure 1A shows the REE concentrations of two calculated parent liquid compositions for Nakhla. Chassigny parent liquids have similar patterns. Nakhla is an unusual rock consisting of large cumulus augite and minor olivine crystals set in a rapidly crystallized matrix (5). The 'closed system' calculation assumes that no net changes in the intercumulus liquid took place after accumulation of the pyroxene, but does allow for partial equilibration of the cumulus crystals and trapped liquid. The 'open system' calculation is a direct calculation based upon the composition of Nakhla augite (6) and the partition coefficients of (7); this calculation allows for the possibility of migration of intercumulus liquid. Both patterns are similar and show dramatic light REE enrichment. This fractionation is truly remarkable in light of the ε_{Nd} value of +16 (6) which requires that the source had a long term pattern of light REE depletion, i.e. something similar to the EETA79001A pattern in Fig. 2B. Compounding the situation is the low Al content of the Nakhla parent liquid (N) evident in Fig. 1 (Pl is the Al bearing component). The Al content is sufficiently low that garnet, which is the most effective REE fractionating agent, cannot have been a residual phase in the parent magma's source region; niether is there much allowance for removal of augite at low pressure. The problem of deriving strongly light-REE enriched magmas from light-REE depeleted source regions is common to terrestrial hot spots, such as Hawaii (8). Single-stage models require prohibitively small degrees of partial melting (<1%), so multi-stage melting models have been invoked to spread the REE fractionation over two or more steps (e.g., 9). Some sort of multi-stage melting process thus seems necessary to explain the Nakhla parent magma composition with the condition that garnet not have been a residual phase in the last stage of melting. In addition to low-Al the Nakhla parent magma also had an unusually high concentration of CaO (~14 wt% (2)). The combination of low-Al and high-Ca requires either that the source was dominated by augite or that CO_2, which has the potential of drastically increasing the CaO content of melts coexisiting with olivine and pyroxene, fluxed the melting at pressures > 25 kb (2). Since partial melting of pyroxene dominated sources produces small negative Eu anomalies in the liquid (10) and since there is no evidence of such an anomaly in Fig. 2A, the presence of CO_2 in martian melting processes must be seriously considered.CO_2 is also an effective carrier of light REE (11), so CO_2 may have affected both trace and major elements during melting.

Fig. 1B illustrates very different REE patterns for the shergottites. The Shergotty pattern is the 70% ICM model taken from (12). The EETA79001A pattern is the bulk rock analysis of (13). EETA79001A is a fine-grained basaltic rock with 10-15 % mafic xenocrysts (14). These xenocrysts will likely have only a minor diluting effect on incompatible elements, so the pattern in Fig. 1B is believed to close to, albeit slightly lower and steeper than, the true parent liquid pattern. The crystallization ages of the shergottites are controversial because of variable shock effects on the isotopic systems and consequentlythe values of ε_{Nd} are model dependent. The values shown in Fig. 1B are consistent with the 180 m.y. age advocated by (15). This age is chosen here because only the younger ages, which yield $\varepsilon_{Nd} > 0$, are petrologically reasonable, and because the 350 m.y. age reported by (16) has been shown to be a mixing line (12). Given these qualifications, the low-Al content, the depleted light-REE pattern, and $+\varepsilon_{Nd}$ of EETA79001A have a straightfoward explanation: partial melting of a low-Al source region with a long term light-REE depletion. In this regard, the source region was similar to that of Nakhla although the EETA79001A magma genesis was apparently much simpler. The ε_{Nd} values for Nakhla and EETA79001A are much higher than typical terrestrial basaltic values, but are more typical of lunar mare basalts. This similarity suggests that Mars was more like the Moon in its ability to maintain long term isotopic heterogeneities in its mantle. Lack of crustal recycling on Mars and/or less vigorous mantle convection than the Earth are probable explanations.

Given the similarity of mineral compositions in Shergotty to those in the groundmass of EETA79001A, it is likely that their parent magmas lay along similar liquid lines of descent, as suggested by Fig. 1, and hence they were derived from similar primary magmas and source regions. If so, then REE pattern and ε_{Nd} of the Shergotty

Shergotty parent magma in Fig. 2B are readily explicable as those of a magma derived from a depleted source region like EETA79001A, but subsequently contaminated by a low-temperature, long-term, light-REE enriched component. The slight U-shape in the light REE is especially indicative of such a contamination. This component probably is crustal, but whether it is older basalt, like the Nakhla parent magma (Fig. 2A), or 'granitic' is not clear; the physics of assimilation favors an evolved composition with a low melting point, however. One thing that is clear is the absence of a negative Eu-anomaly in the Shergotty REE pattern. Consequently, this crustal component was unlike lunar KREEP, which has a prominent negative Eu-anomaly (17).

Fig. 2A contains REE concentrations for the Nakhla parent ('closed system') and the bulk data for EETA79001A taken from Fig. 1 plus additional calculated and measured concentrations of some high-field-strength elements (HFSE) arranged in order of incompatibility. Fig. 2A shows that there are complementary anomalies for Ta, Hf, and Zr in the Nakhla and EETA79001A patterns, thus supporting the hypothesis that the shergottites were generated by remelting a source depleted in a Nakhla-like component. Fig. 2B schematically illustrates typical incompatible element patterns for basalts from terrestrial oceanic islands (OIB), volcanic arcs (ARC), and mid-ocean ridges (MORB). Despite the fact that there is no evidence of plate tectonics on Mars, the Nakhla parent magma pattern appears more similar to the ARC pattern than to OIB or MORB. This similarity is probably due to similar fractionations of the REE from the HFSE during transport by a CO_2-rich vapor phase, rather than similar tectonic styles.

REFERENCES: (1) McSween, H. Y. (1985) *Revs. Geophys., 23*, 391-416. (2) Longhi, J. and Pan, V. (1989) *Proc. Lunar Planet. Sci. Conf. 19th*, p. 451-464. (3)Toulmin, P., III, Baird, A. K., Clark, B. C., Keil, K., Rose, H. J., Jr., Christian, R. P., Evans, P. H., and Kelliker, W. C. (1977) *J. Geophys. Res. 82*, 4625-4634. (4) Bertka, C. M. and Holloway, J. R. (1988) *Proc. Lunar Planet. Sci. Conf. 18th*, 723-739. (5) Treiman A. H. (1986) *Geochim. Cosmochim. Acta, 50*, 1061-1070. (6) Nakamura, N., Unruh, D. M., Tatsumoto, M. and Hutchinson, R. (1982) *Geochim. Cosmochim. Acta, 46*, 1555-1573. (7) McKay G., Wagstaff J., and Yang S.-R. (1986) *Geochim. Cosmochim. Acta, 50*, 927-937. (8) Chen C.-Y. and Frey F.A. (1985) *J. Geophys. Res., 90*, 8743-8768. (9) Ribe N.M. (1988) *Earth Planet. Sci. Lett., 88*, 37-46. (10) Shearer C.K. and Papike J.J. Proc. (1989) *Lunar and Planet. Sci. Conf. 20th*, in press. (11) Wendlendt R.F. and Harrison W.J. (1979) *Contrib. Minerl. Petrol., 69*, 409-419. (12) Lundberg L.L, Crozaz G., McKay G., and Zinner E. (1988) *Geochim. Cosmochim. Acta, 52*, 2147-2163. (13) Burghele A., Dreibus G., Palme H., Rammensee W., Spettel B., Weckwerth G., and Wanke H. (1983) *Lunar Planetary Science XIV*, 80-81. (14) McSween H.Y. and Jarosewich E. (1983) *Geochim. Cosmochim. Acta, 47*, 1501-1513. (15) Jones J.H. (1986) *Geochim. Cosmochim. Acta, 50*, 969-977. (16) Jagoutz, E. and Wänke, H. (1986) *Geochim. Cosmochim. Acta, 50*, 939-953. (17) Warren P. H. and Wasson J.T. (1979) *Rev. Geophys. Space Phys., 17*, 73-88.

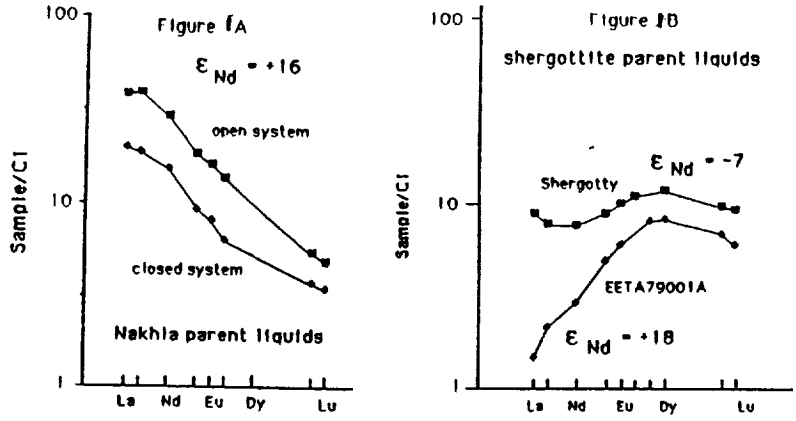

Figure 1. REE in Nakhla and shergottite parent magma compositions. Nakhkla - calc.,this study; Shergotty - calc(12); EETA79001A - bulk (13).

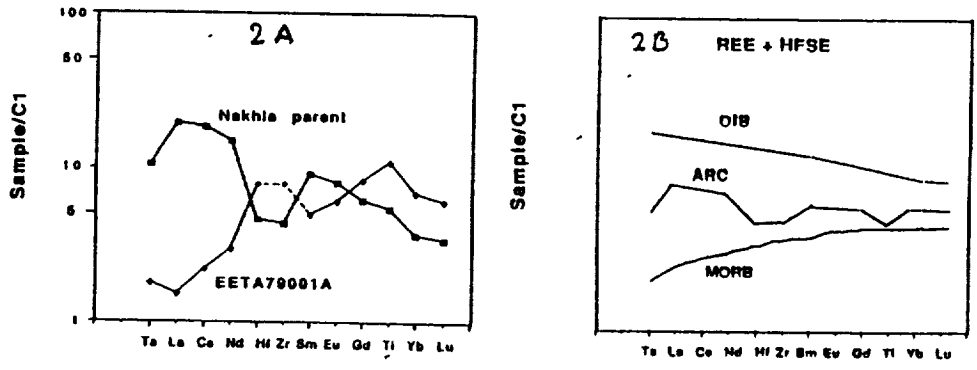

Fig. 2 A. Calculated REE and HFSE in Nakhla parent magma and bulk EETA79001A. B. Typical (schematic) patterns for terrestrial basalts.

VALLES MARINERIS, MARS: ARE PIT CHAINS FORMED BY EROSION AND TROUGHS BY TECTONISM?; B.K. Lucchitta, R.A. Balser, and L.M. Bertolini, U.S. Geological Survey, Flagstaff, AZ 86001.

The origin of the Valles Marineris remains controversial. Erosional [1], tectonic [2], and hybrid processes [3] have been proposed. Erosional processes appeared attractive because a morphologic continuum was thought to exist from pit chains of probable erosional origin to larger troughs. Schultz [4], however, refuted the existence of this continuum. To clarify these contradictions, we compared the widths and depths of pit chains and troughs and found that the features do not form a continuum. Rather, results are consistent with the hypothesis that pit chains formed by surficial collapse and troughs by deeper seated and coherent failure.

We classified by inspection all pit chains and linear depressions in the Valles Marineris region into six morphologic categories: (1) pit chains (linear arrays of small pits), (2) floored chains (arrays of pit chains having flat or hummocky floors), (3) scalloped troughs (wider linear depressions with scalloped wall segments), (4) narrow troughs (depressions of intermediate width with straight wall segments), (5) wide troughs (broad, linear depressions), and (6) chaotic troughs (more irregular depressions displaying some channel morphologies). We drew topographic profiles across the classified depressions at each degree of longitude between long 45° and 90°, on the basis of 1:2,000,000-scale topographic maps of MC 18 NW [5] and 18 NE and SE (work in progress). For each profiled depression, we determined the erosional width between plateau margins, the depth from the surrounding plateau level to the deepest part, and the geologic unit (modified from Witbeck et al. [6]) exposed at the deepest point.

Depths and widths are shown in Figs. 1 and 2. Fig. 1 shows measurements of all troughs. Fig. 2 is the same but with omissions of three types: (1) chaotic troughs, which are genetically linked to outflow channels; (2) troughs east of long 61°, which are transitional to chaotic troughs; and (3) troughs whose maximum depth is not likely to reflect the approximate structural depth because of thick fill from landslides or interior deposits.

Results of the study, as deduced from the figures, are as follows:

1. Pit chains, floored chains, and scalloped troughs lie along a continuously ascending trend that suggests a common origin. Surficial erosional collapse into linear subsurface voids or tension cracks [3] is compatible with this observation. The limiting depths of about 4 km may be due to a discontinuity at that depth or to restricted size of the underlying voids.

2. Narrow and wide troughs form a continuum that suggests their formation by similar processes. The straight scarps bordering these troughs suggest control by faulting rather than surficial collapse.

3. A gap in data occurs at widths of 20-35 km, separating pit chains, floored chains, and scalloped troughs from narrow and wide troughs. Only two transitional points are located within this gap. The gap suggests an abrupt change in physical conditions or processes. Apparently, deep-seated, more coherent failure was activated for troughs wider than about 35 km.

4. Most troughs bottom out at 8-9 km regardless of width, perhaps implying a controlling discontinuity or limit in the amount of extension.

REFERENCES

[1] McCauley, J.F., M.H. Carr, J.A. Cutts, W.K. Hartmann, Harold Masursky, D.J. Milton, R.P. Sharp, and D.E. Wilhelms (1972) Icarus 17, 289-327. [2] Blasius, K.R., J.A. Cutts, J.E. Guest, and Harold Masursky (1977) Jour. Geophys. Res. 87, 9723-9733; [3] Tanaka, K.L. and M.P. Golombek (1989) Proc. 19th Lunar and Planet. Sci. Conf., 383-396; [4] Schultz, R.A. (1989) MEVTV Workshop on Tectonic Features on Mars, 21-22; [5] U.S. Geological Survey (1986) U.S. Geol. Surv. Misc. Inv. Map I-1712; [6] Witbeck, N.E., K.L. Tanaka, and D.H. Scott (in press) U.S. Geol. Surv. Misc. Inv. Ser. Map I-2010.

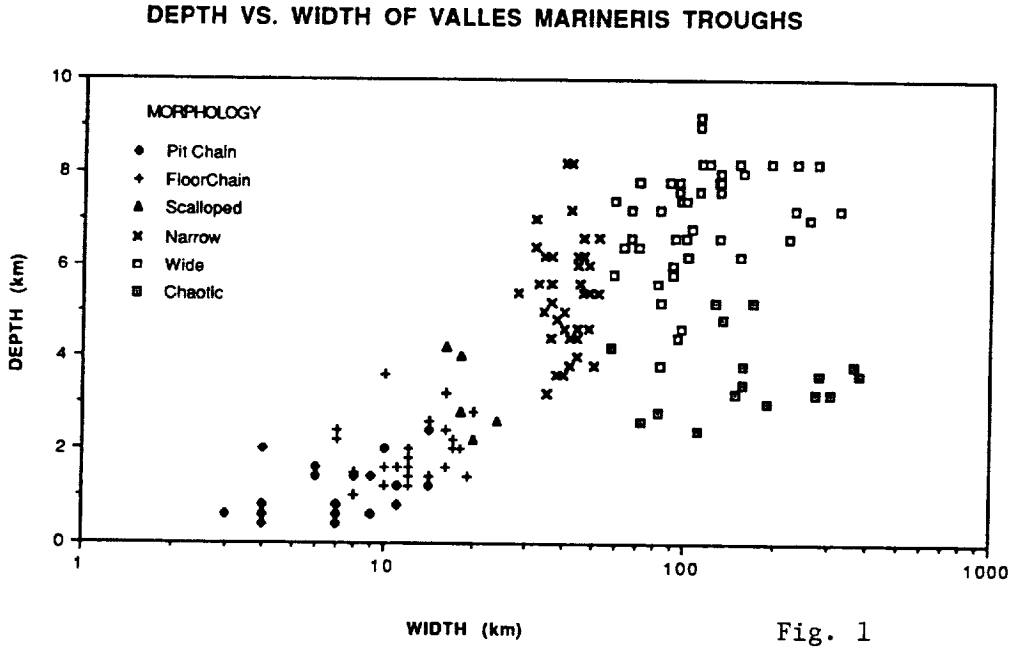

Fig. 1

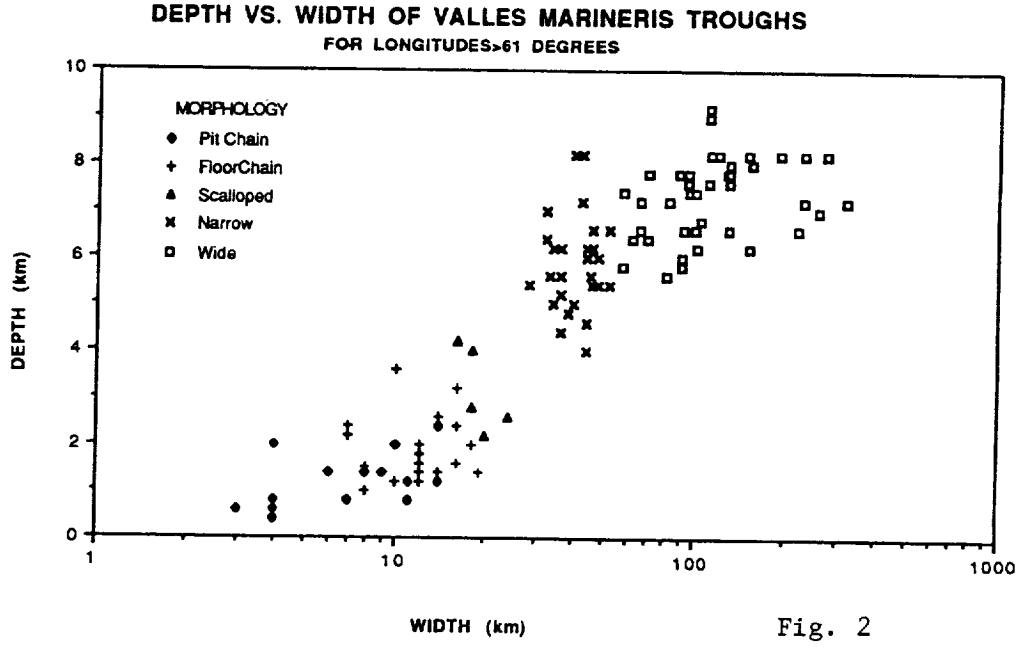

Fig. 2

A PHYSICAL MODEL OF THE IMPACTED MARTIAN CRUST: HYDROLOGIC AND MECHANICAL PROPERTIES AND GEOLOGIC IMPLICATIONS; *David J. MacKinnon and Kenneth L. Tanaka, U.S.G.S., 2255 N. Gemini Dr., Flagstaff, AZ 86001*

Photogeologic evidence suggests a close association of many outflow [1,2], intermediate [3], and sapping [4] channels with regions affected by uplift, fracturing, and geothermal heating [1, 5]. The magnitude and diverse morphology of the channeling are impressive by terrestrial standards, especially because there is little evidence that significant rainfall has occurred on Mars [6]. By the end of the heavy bombardment, outgassed water probably had been emplaced in the upper crust [7]. Nearly all the channels originated from or are associated with ancient cratered terrain, some of which has been resurfaced by lava flows and eolian processes. Because high impact fluxes during bombardment probably fragmented most of the materials that resurfaced the impacted surface, we believe that a simple physical and structural model of the impacted, ancient cratered terrain can reasonably describe physical properties fundamental to interpreting subsequent channel formation, as well as other geologic activity.

On this basis, we developed a two-layer model for the impacted crust: an ejecta (impact breccia) zone overlying a zone of fractured basement rock [see 8, 9]. The proposed ejecta zone is 1 to 2 km thick and consists of well-mixed, very poorly sorted impact breccia that grades into the fractured zone. The fractured zone is composed of meter-size or larger blocks of basement rock, and it extends to the depth of lithostatic closure (10 km or more, depending on pore-water pressure [10]). The porosity and permeability of these zones depend on the size distribution and packing of the breccia and fractured blocks. From the results of measurements from terrestrial impact and explosion craters, laboratory analyses, and experimentally verified theoretical models for porosity and permeability, we determined that in such an impacted crust, clast size and degree of sorting increase with depth. These trends cause (1) porosity to decrease with depth throughout the affected crust, (2) permeability to increase with depth to the top of the fractured zone and then to decrease as fracture width and frequency decrease with depth, and (3) material strength to increase with depth from cohesionless to that of solid bedrock. Extrapolating from typical size distributions and packing among ejecta and fractured blocks, we estimate the porosity of the ejecta zone as 10-20 percent and the porosity of the upper part of the fractured zone as less than a few percent; the permeability of the ejecta zone would be less than 0.01 darcys, and the permeability of the upper part of the fractured zone would be about 1000 or more darcys.

We recognize two major limitations of our model: (1) few terrestrial impact and explosion craters provide empirical data for the analysis of the effects of single and multiple impacts on rock structure, and (2) the subsurface stratigraphy of Mars is poorly known. Thus some of our basic assumptions are speculative, allowing for different possibilities regarding the nature of the Martian crust. In one alternative view [10], the crust is more heterogeneous than we have portrayed; thus its hydraulic properties may be more varied, and impact fractures in the basement rocks, if filled, would appreciably lower the bulk permeability.

In spite of such problems, we feel that our two-layer model is generally valid, because it can account for a great diversity of Martian geologic phenomena. Photogeologic evidence suggests mechanical discontinuities in the Martian crust at 1- to 3-km depths, which in some places may form the contact between the ejecta and the fractured zones. Generally, lower layers of the ancient crust have progressively greater resistance to erosion. Within the deeply eroded Kasei Valles, for example, erosional discontinuities in the

channels are evident at depths of 1.0 and 2.6 km. The upper discontinuity has been interpreted as the ejecta/basement contact [11], the interface between ice-laden and dry or wet regolith [12], or the zone between pristine and cemented regolith [13]; the lower discontinuity is consistent with the depth to the base of sapping channels along the Valles Marineris and has been interpreted as the ejecta/basement contact [12]. Such discontinuities are consistent with observed graben widths and collapse pits proposed to originate by collapse of cohesionless material into tension fractures at depth in basement rocks [12, 14].

The Chryse channels may be explained by high pore pressures and fluidization of the base of the ejecta zone by the fractured zone, causing enormous retrogressive debris flows [15]: after removal of the overburden, floods from the fractured zone could have easily eroded ejecta-zone breccia. Late-stage debris flows, sapping channels, and landslides along the channel margins completed the morphology seen today. If debris flows played a central role in the formation of the large outflow channels, their mobilization would require much less water [16] than the flood model [7]. The breccia of the ejecta zone is poorly sorted and rich in clay-size particles, analogous to the clast distributions of terrestrial debris flows [9]. An explanation for the great runout distances of debris flows over very low gradients, however, has not yet been offered.

Other geologic features consistent with our model include (1) outflow channels produced by catastrophic floods erupted from joints or faults that tap the fractured zone and act as high-volume conduits [13,17]; (2) sapping channels where the permeability of the ejecta zone was sufficient to promote sapping of exposed, saturated ejecta; (3) chaotic terrain, possibly formed by liquefaction of breccia at depths of hundred of meters to more than a kilometer [18]; (4) complex channels such as Nirgal Vallis, which can be explained as a combination of outflow along a tension fracture that taps the fracture zone (lower part of channel) and sapping from the ejecta zone (upper part of channel); and (5) high-latitude debris aprons and channels with modest wall slopes (e.g., Auqakuh Vallis) composed of ice-rich impact breccia of low yield strength [19].

Our physical model for the ancient, impacted Martian crust, coupled with local volcano-tectonic histories, enables a more complete understanding of the formation of many common geologic features on Mars. Previously, catastrophic flood models have not addressed the dependence of permeability on clast and fracture distributions and the cohesion of the cratered terrain material, and debris-flow models have not addressed the physical mobility of the material. Furthermore, the ejecta/fractured zone stratigraphy explains many observations of Martian erosional and structural discontinuities.

References:

[1] Tanaka, K.L. and MacKinnon, D.J. (1987) (abs.) LPSC 18, 996-997;[2] Tanaka, K.L. and Chapman, M.G. (in press) PLPSC 20;[3] MacKinnon, D.J. and Tanaka, K.L. (1987) (abs.) LPSC 18, 588-589;[4] Kochel, R.C. and J.F. Piper (1986) JGR 91, E175-E192;[5] Mouginis-Mark, P.J. (1985) Icarus 64, 265-284;[6] Pieri, D.C. (1980) NASA TM 81979, 1-160;[7] Carr, M.H. (1979) JGR 84, 2995-3007;[8] MacKinnon, D.J. and Tanaka, K.L. (1987) (abs.) LPSC 19, 707-708;[9] MacKinnon, D.J. and Tanaka, K.L. (1989) JGR 94, 17,359-17,370;[10] Clifford, S.M. (1984) Ph.D. dissertation, U of Mass., 285 p;[11] Robinson, M.S. and Tanaka, K.L. (1987) (abs.) LPI Tech. Rep. 88-05, 106-108;[12] Davis, P.A. and M.P. Golombek (in press), JGR, MEVTV Special Issue;[13] Soderblom, L.A. and D.B. Wenner (1978), Icarus 34, 622-637;[14] Tanaka, K.L. and Golombek, M.P. (1989) PLPSC 19, 383-396;[15] Numedal, D. and D.B. Prior (1981) Icarus 45, 77-86;[16] Rodine, J.D. and A.M. Johnson (1976) Sedimentology 23, 213-234;[17] Tanaka, K.L. and MacKinnon, D.J. (1989) (abs.) 4th Mars Conf., 200-201;[18] Tanaka, K.L. (1987) (abs.) LPSC 19, 1175-1176;[19] MacKinnon, D.J., Tanaka, K.L., and Winchell, P.J. (1987) (abs.) LPI Tech Rep. 88-05, 82-85.